PART V

SYSTEM PERFORMANCE EVALUATION AND CONCLUSIONS

CHAPTER ELEVEN

SYSTEM VERIFICATION AND PERFORMANCE EVALUATION

11.1 INTRODUCTION

This chapter compares the system performances of the balanced and dual channel DSSS QPSK modulation configurations, employing a class of constant-envelope root-of-unity (CE-RU) filtered complex spreading sequences, with conventional Nyquist filtered QPSK modulated CDMA systems employing binary spreading sequences. A verification and performance evaluation of the balanced and dual channel DSSS QPSK system employing CSS are presented in terms of bit error rate performance, spectral and power efficiency, transmitter output peak-to-average power ratio (PAPR), etc.

The comparison is also done in non-linear power amplification and is based on Complementary Cumulative Probability Density Function Peak-to-Average Power Ratio (CCDF-PAPR) measurements, as well as the amount of spectral regrowth experienced when the power amplifier is driven close to the so-called $1dB$ saturation point. Simulation as well as hardware results are presented to illustrate the superiority of the new complex-spreaded WCDMA modulation schemes over conventional methods in terms of spectral and power efficiency in the presence of non-linear power amplification.

The importance of nonlinear amplifier effects in communication systems design is supported by a number of research studies that have been conducted on this topic. Liang *et al* [47] investigates the tradeoffs between amplifiers and modulation waveforms in complex digital communication systems and introduces a figure-of-merit whereby a better understanding of the relations between amplifier efficiency, amplifier distortion, signal to in-band and adjacent channel interference, and power consumption may be obtained.

The effect of different input drive levels of the amplifier on the in-band distortion, as well as adjacent channel interference (ACI) due to spectral regrowth are quantified. In [48] analytical results are presented on spectral regrowth of modulation schemes, which are useful in finding optimal operating conditions of the power amplifier (PA) to achieve maximum efficiency without violating the out-of-band emission requirement.

11.2 BER PERFORMANCE MEASUREMENTS

11.2.1 Signal-to-Noise Ratio

As stated in [49], when there is only one transmitter in operation, the receiver performance can only be limited by noise. If it is assumed that the externally caused interference (ECI) is negligible, the total noise power P_N in the receiver bandwidth is

$$P_N = k \cdot T \cdot B_N \cdot NF \tag{11.1}$$

where

k = Boltzman's constant ($-228.6 dBW sec/^oK$ or 1.380 x $10^{-23} J/^oK$)

T = Absolute temperature in degrees Kelvin

B_N = Double-sideband noise bandwidth of the receiver

NF = Noise figure of the receiver

At a room temperature of 17^oC (290^oK), the parameter $kT = -174 dBm/Hz$.

The bit energy-to-noise density, E_b/N_o, ratio is an important parameter for the performance evaluation and comparisons between different systems. In practical systems it is more convenient to measure the average received signal-to-average noise power ratio, (P_S/P_N). The following relations for converting from E_b/N_o to P_S/P_N, as given in [49], are

$$E_b = P_S \cdot T_b = P_S \left(\frac{1}{f_b} \right) \tag{11.2}$$

$$N_o = \frac{P_N}{B_N} \tag{11.3}$$

$$\frac{E_b}{N_o} = \frac{P_S \cdot T_b}{P_N / B_N} = \frac{P_S / f_b}{P_N / B_N} = \frac{P_S \cdot B_N}{P_N \cdot f_b} \tag{11.4}$$

$$\frac{E_b}{N_o} = \frac{P_S}{P_N} \cdot \frac{B_N}{f_b} \tag{11.5}$$

Thus, the ratio E_b/N_o is the product of the P_S/P_N ratio and the receiver noise bandwidth-to-bit rate ratio (B_N/f_b).

In the case of a DSSS communication system the receiver noise bandwidth, B_N, can be expressed in terms of the chip rate, f_{chip}, as

$$B_N = x \cdot f_{chip} \tag{11.6}$$

where normally $x < 1$. Equation 11.5 can therefor be rewritten as

$$\frac{E_b}{N_o} = \frac{P_S}{P_N} \cdot x \cdot \frac{f_{chip}}{f_b} \tag{11.7}$$

Given that the processing gain (PG) of the DSSS system is defined by

$$PG = \frac{f_{chip}}{f_b} \tag{11.8}$$

Equation 11.7 becomes

$$\frac{E_b}{N_o} = \frac{P_S}{P_N} \cdot x \cdot PG \tag{11.9}$$

The E_b/N_o ratio in Equation 11.9 can be presented in terms of decibels (dB) as

$$\frac{E_b}{N_o}[dB] = \frac{P_S}{P_N}[dB] + 10\log x + 10\log PG \tag{11.10}$$

The first step in evaluating the DSSS communication system, employing CSS, was to perform bit error rate (BER) tests. The output of the DSSS transmitter, modulated onto an $850\ MHz$ IF frequency, is attenuated to the appropriate power levels for the tests by means of a variable attenuater. The attenuated output is then produced as input to an Hewlett Packard (HP) noise test set, which adds AWGN to the signal for a given $\frac{E_b}{N_o}$ value. The signal plus AWGN forms the input to the DSSS receiver, which demodulates, despreads and differential decode the signal to recover the original transmitted data. A BER analyser is used to perform the bit error probability test, comparing the transmitted data stream with the recovered data stream at the receiver.

Figure 11.1 depicts the BER of the hardware implemented differential encoded balanced/dual DSSS QPSK system employing CSS compared to the BER of theoretical QPSK and differential encoded QPSK. The hardware implementation loss of the DSSS system is in the order of $1.5\ dB$, compared to that of theoretical differential encoded QPSK.

The complete DSSS system was simulated and BER results were obtained. The simulated BER result, in the presence of AWGN, is shown in Figure 11.2.

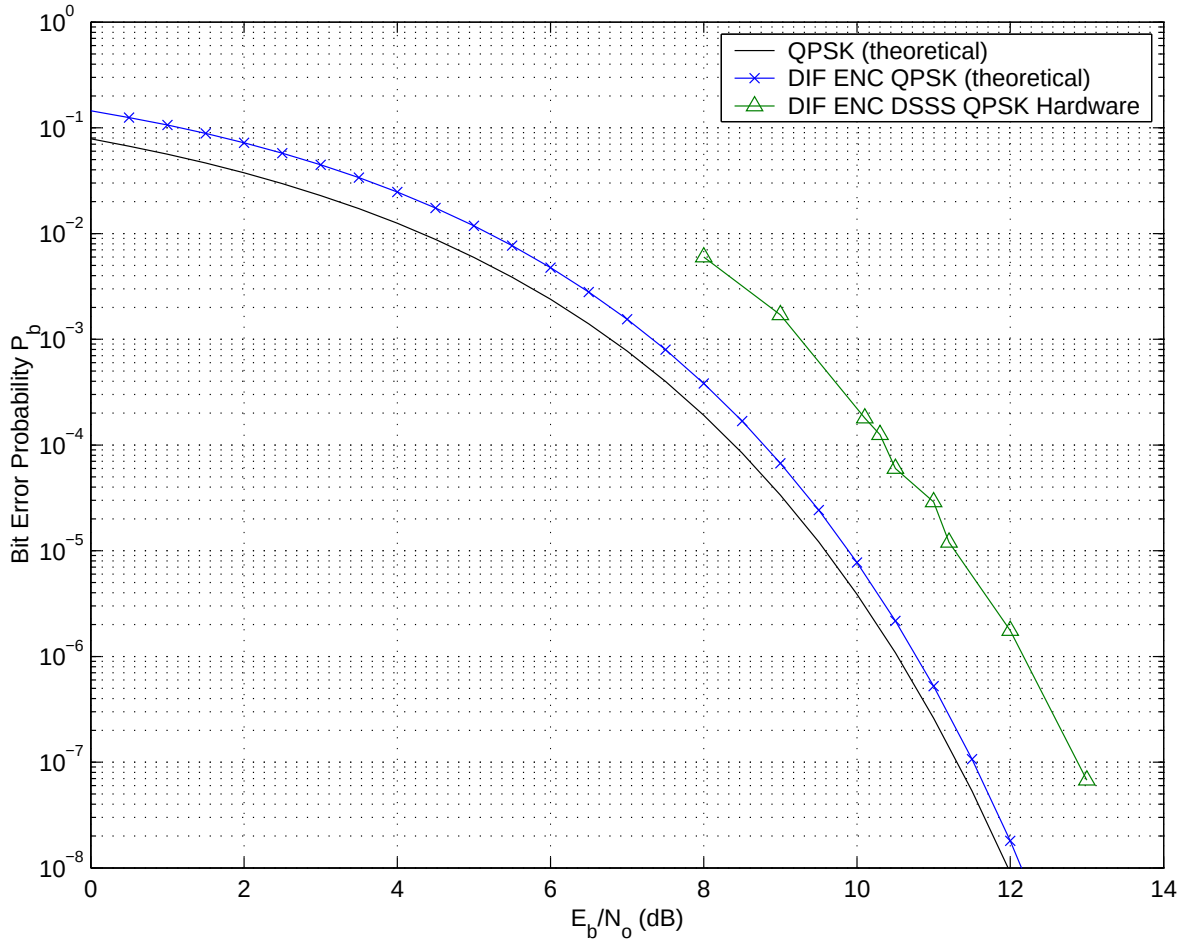

FIGURE 11.1: Bit error probability of the hardware implemented differential encoded balanced/dual DSSS QPSK system employing CSS compared to BER of theoretical QPSK and DE theoretical QPSK

The system was also simulated to investigate the effect of different phase errors on the BER performance of the DSSS system. Figure 11.4 shows the BER of the dual channel DSSS QPSK system with different phase errors between transmit and receive quadrature carriers. This result can be compared to the BER performance of a theoretical QPSK communication system also with different phase errors between transmit and receive carriers as shown in Figure 11.3. The simulated BER results corresponds with the theoretical BER results for specific phase errors.

A Motorola channel simulator, written in C++ language, was used to do system simulations in a Raleigh-faded and AWGN channel. The simulated BER result obtained is compared with the corresponding BER result of a theoretical QPSK system in an AWGN and Raleigh-faded channel, as depicted in Figure 11.5.

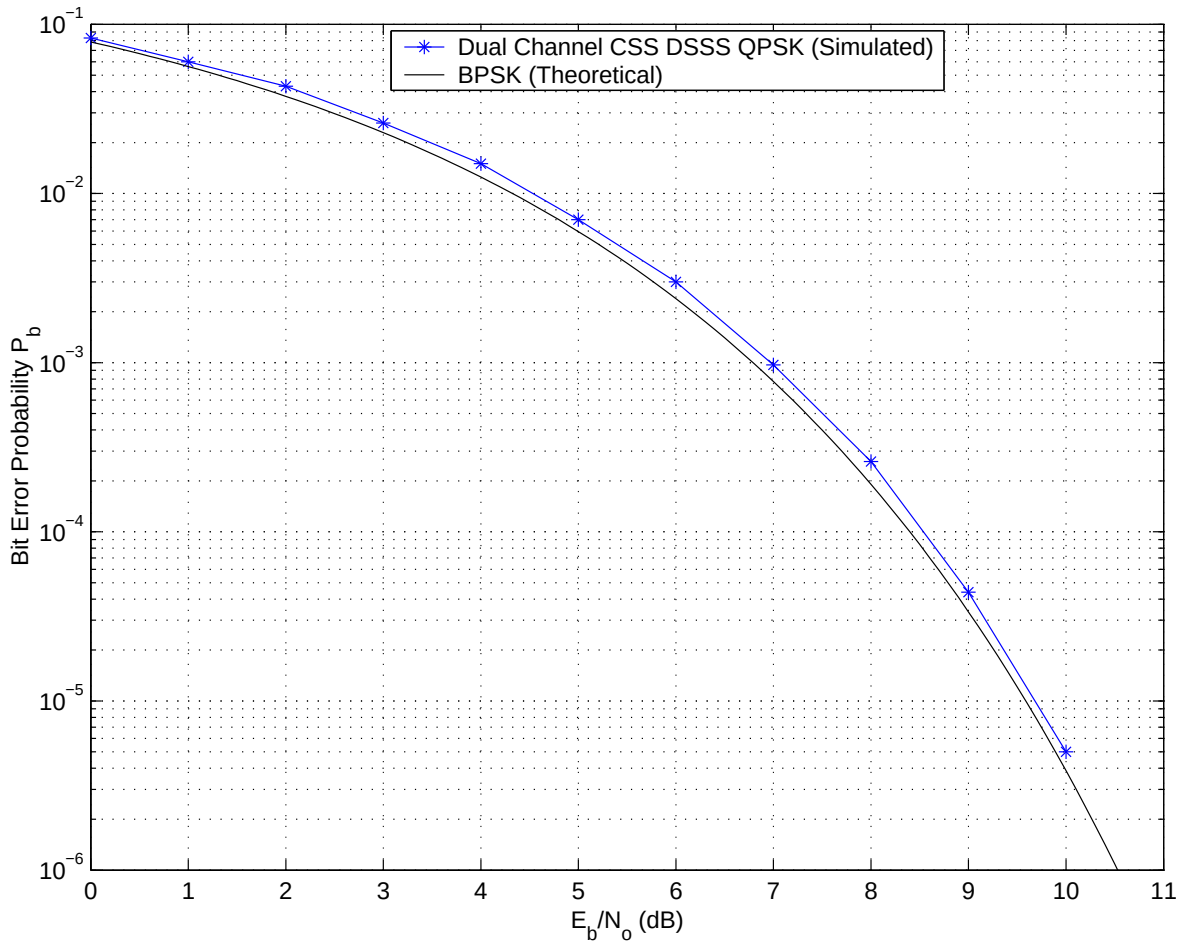

FIGURE 11.2: Bit error probability of the simulated balanced/dual DSSS QPSK system employing CSS compared to BER of theoretical QPSK

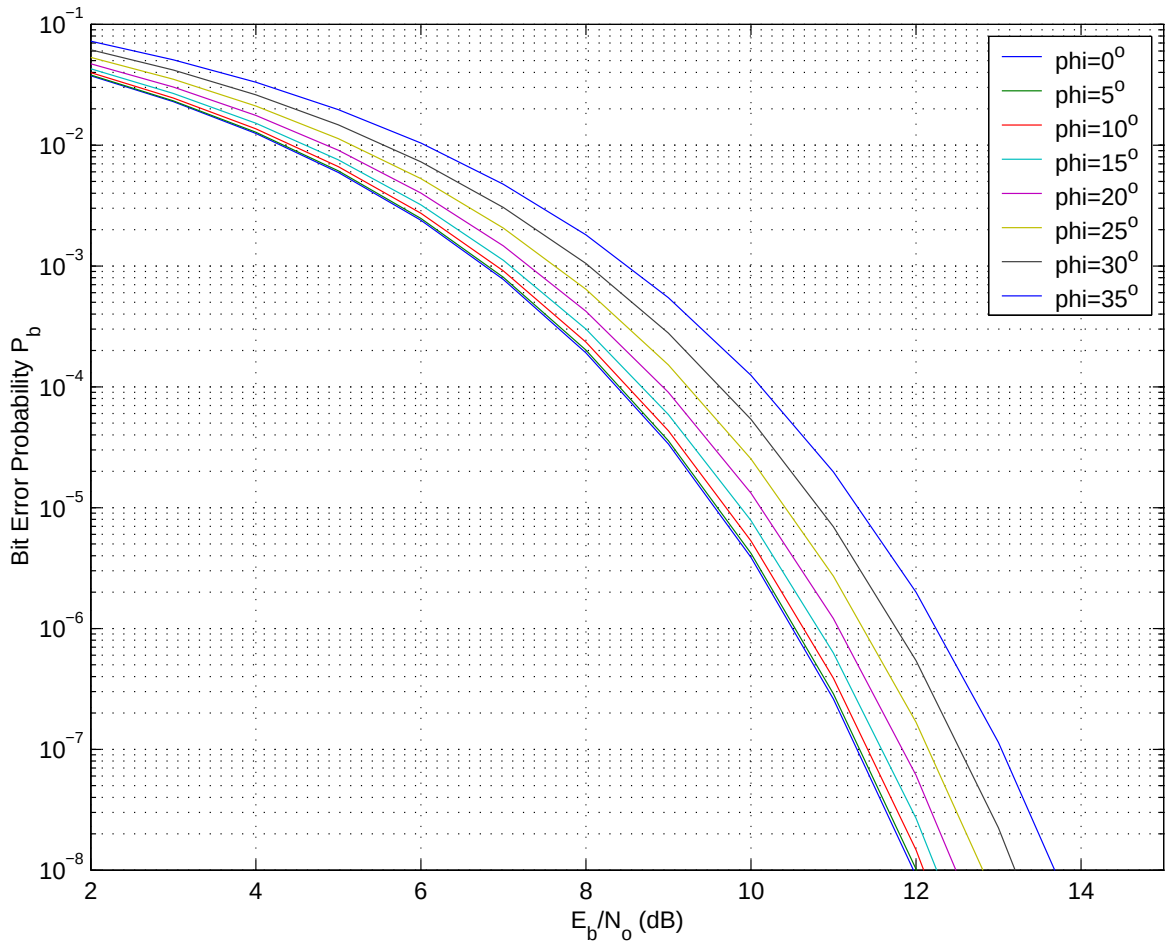

FIGURE 11.3: Bit error probability of a theoretical QPSK communication system with different phase errors between transmit and receive quadrature carriers

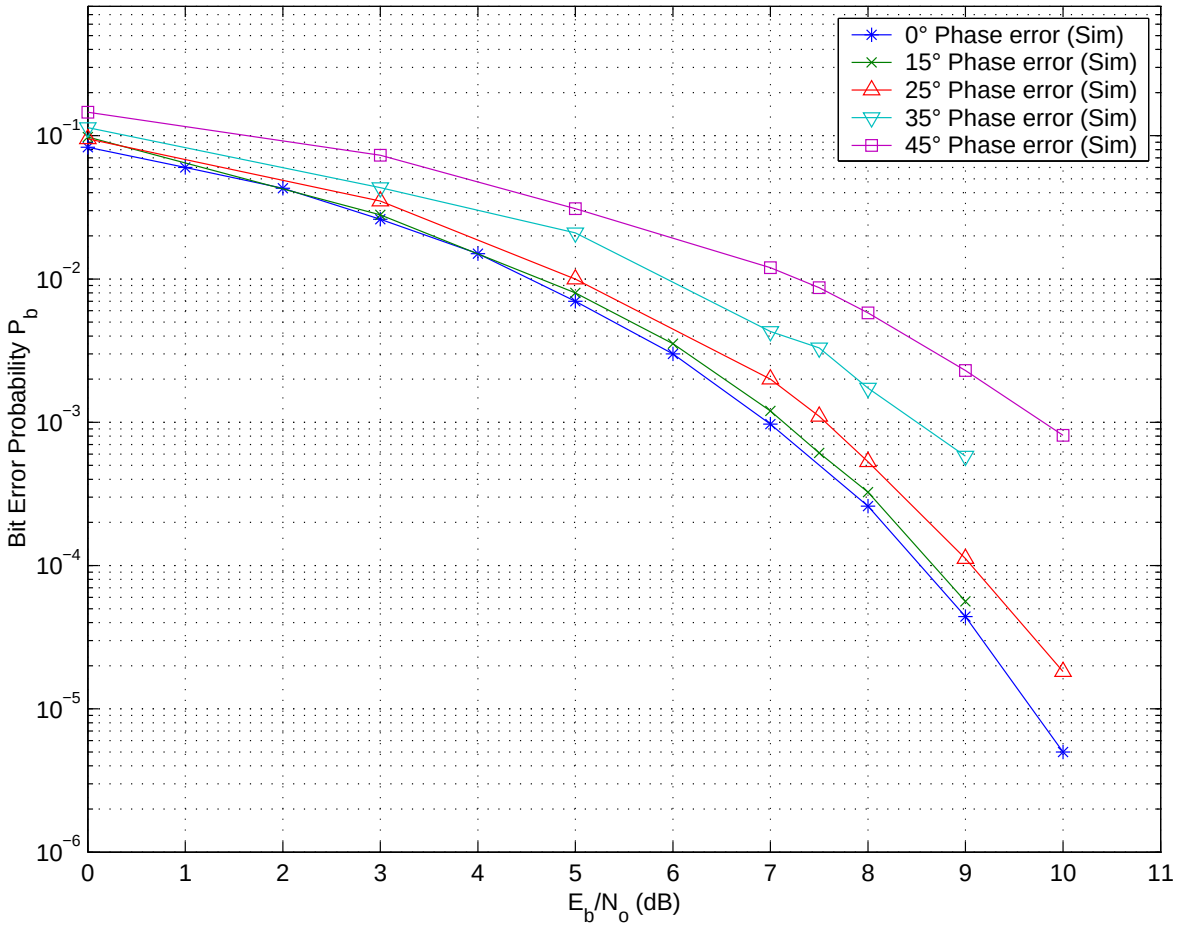

FIGURE 11.4: Bit error probability of the dual channel DSSS QPSK system employing CSS with different phase errors between transmit and receive quadrature carriers

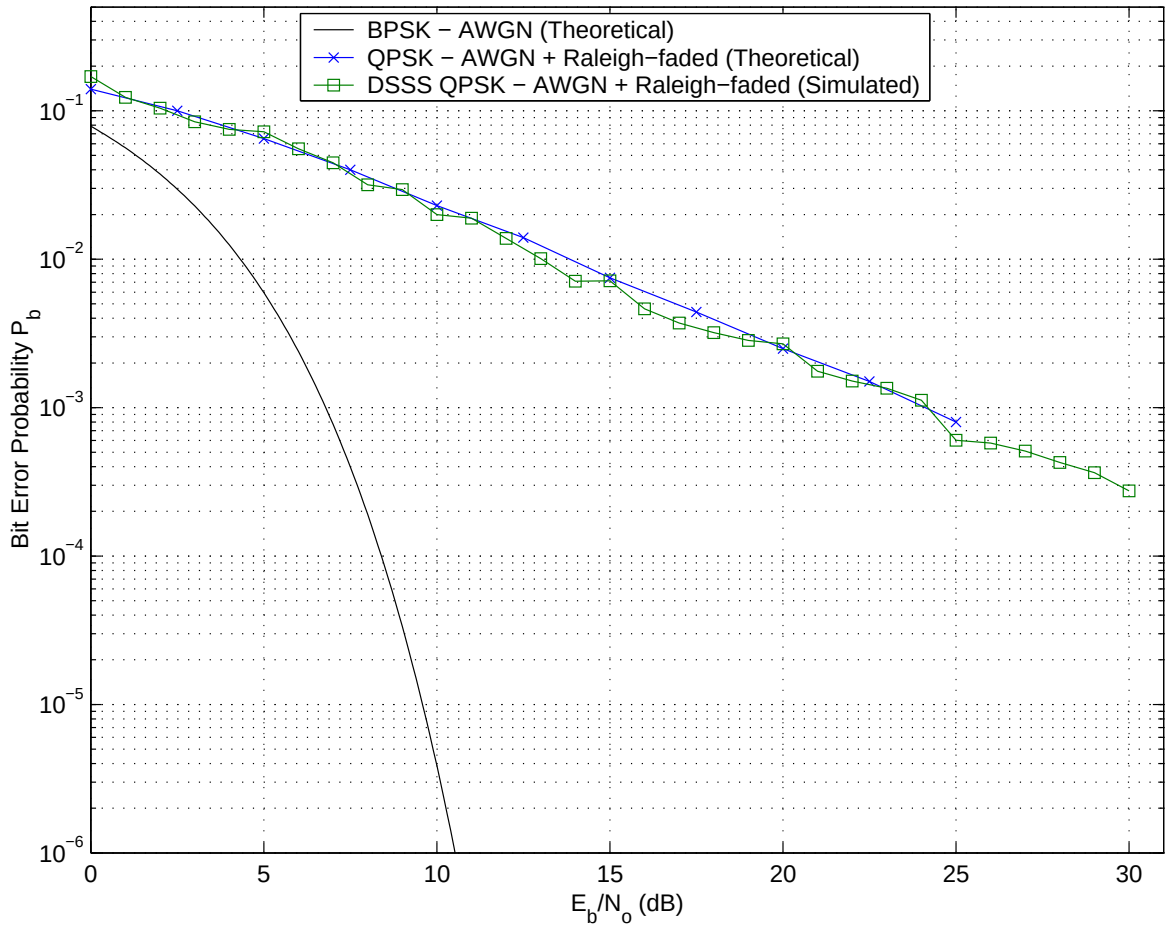

FIGURE 11.5: Bit error probability of the simulated balanced/dual DSSS QPSK system employing CSS in an AWGN and Raleigh-faded channel compared to BER of theoretical QPSK in an AWGN and Raleigh-faded channel.

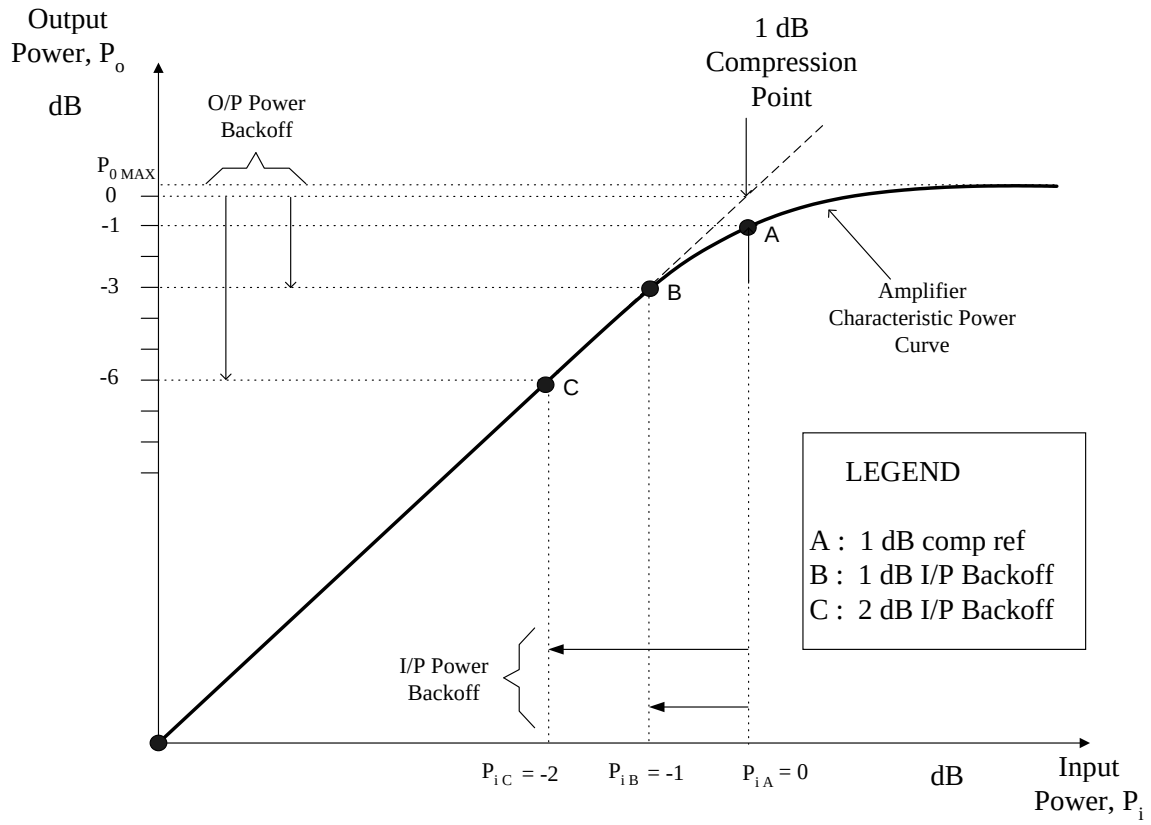

FIGURE 11.6: Typical theoretical High Power Amplifier (HPA) input/output power saturation characteristic curve

11.3 POWER SATURATION PERFORMANCE

Power amplification constitutes one of the most important processes in modern cellular communication systems. Since the power amplifier provides the transmit signal levels needed to overcome the path loss between the transmitter and receiver, and may consume a significant fraction of the power used by the system, it plays a crucial role in the definition of battery life in the design of mobile communication systems. Furthermore, apart from the power source (battery pack), it turns out to be the single most expensive component in portable telephone handsets. Since the power amplifier is an active device, it is subject to non-linear effects that can add noise and cause signal distortion. The amplifier efficiency increases with increasing input power, thus, a system-level tradeoff exists between power efficiency or battery life and the resulting distortion introduced when power amplifiers are driven close to their so-called *1dB saturation* or *1dB compression point* (see Figure 11.6).

To keep costs down without sacrificing system performance, power amplifiers have to be designed for optimum power amplification efficiency. Several system parameters dictate the choice of a specific amplifier configuration, which may be class A, A-B, B or C. Firstly, it is

well known that the power efficiency of class B amplifiers are in the order of 70%, whereas the power efficiency of class A amplifiers are considerably $(\pm 40\%)$ lower and in the order of 30%. Significant power savings are therefore incurred if linear amplifiers can be replaced by non-linear devices. Secondly, the degree of amplifier linearity required for a particular application is primarily dictated by the modulation scheme employed. Class A amplifiers are mostly chosen in cases where a high degree of linearity is required, whereas the operation of class B and C amplifiers are known to be non-linear. As a rule linear amplification methods are preferred when modulation schemes with large amplitude variations are employed, while non-linear amplification methods such as class B or C configurations may suffice in the case of so-called constant-envelope modulation schemes. An example of the latter is Minimum Shift Keying (MSK), which is the chosen modulation scheme in the Global System for Mobile (GSM) Communication cellular modulation standard.

The power efficiency of modulation schemes are usually measured in terms of the peak-to-average power ratio (PAPR) characteristics exhibited by the modulator output signal. This parameter defines the headroom required in linear amplifiers to prevent clipping or compression of the modulated carrier. When this quantity approaches one, the modulation method is relatively insensitive to power (envelope) saturation. This insensitivity is measured or sensed in terms of the degree of spectral regrowth experienced during saturation. It is well known that constant envelope modulation schemes exhibit very little, if any, spectral regrowth under non-linear amplification (saturation). Not only may non-linear amplifiers be employed in these cases, but even larger power efficiency may be achieved by allowing the power amplifier to operate closer to the amplifier 1dB saturation point, without causing excessive spectral regrowth. This chapter investigates the tradeoffs between modulation and power amplifier nonlinearity and efficiency, the goal being to minimize the energy required to communicate WCDMA-modulated digital information in an adverse mobile communication environment.

In the system evaluation in this chapter a statistical approach to power amplifier PAPR measurements is taken. In particular, Complementary Cumulative Distribution Function (CCDF) results are presented. The CCDF expresses the probability that the power is greater than a specified power value. The CCDF of two patented near Constant Envelope (CE) WCDMA modulation configurations employing complex spreading sequences, henceforth referred to as ”1/2C” and ”1C”, respectively, is presented [50] and [51]. The results are compared to a Nyquist filtered QPSK reference system, resembling the binary pilot channel specified in the WCDMA standards [52]. QPSK has been chosen as the reference

system, firstly to facilitate direct comparison with a diverse variety of theoretical and practical modulation schemes, and secondly by virtue of its universal application in a host of applications, including the UMTS [53] and 3GPP WCDMA standards.

11.3.1 Peak-to-Average Power Ratio (PAPR) Complementary Cumulative Distribution Function

In a non-statistical peak power measurement the peak-to-average power ratio (PAPR) is easy to visualise in the case of simple modulation schemes in which there are close correspondence between the modulating waveform and the carrier envelope. In the absence of this correspondence, the PAPR alone does not provide adequate information. This is particularly true with digital modulation methods in which amplitude and phase modulation are combined in a multi-level arrangement, resulting in signal envelopes which are a complex function of the data stream content, rather than the amplitude of the modulating signal. In these cases the resulting signal envelope cannot be directly related to modulation parameters such as modulation depth and modulation index.

The resulting noise-like character of these signals suggests a statistical approach to peak and average power analysis.

Let Y be a discrete random variable (rv) with a range equal to all possible sampled values of peak-to-average carrier power. Then y denotes a specific power value contained in Y. Let PDF denote the probability distribution function of Y. Then PDF is the percentage of time that the PAPR is equal to or smaller than a specific value, y. PDF expressed as a percentage is

$$\text{PDF} = P(y) = 100 \times P(Y = y) \tag{11.11}$$

where y ranges over all values in Y, $0 \leq P(y) \leq 100\%$. The PDF, and specifically the envelope PDF, is useful for analysing the nature of modulating signals. Sustained power levels such as the flat tops of pulses or steps will show up as spectral peaks or lines. Random noise will produce a smooth Gaussian shaped curve.

Let CDF denote the cumulative distribution function of Y. The CDF is the probability that the PAPR is less than or equal to a specific value, y. The CDF is non-decreasing in y, that is, the graph of CDF versus y cannot have negative slope. The maximum PAPR sample taken will lie at 100%. CDF expressed as a percentage is

$$\text{CDF} = Q(y) = 100 \times P[Y \leq y] \tag{11.12}$$

where y ranges over all values in Y, $0 \leq Q(y) \leq 100\%$ $Q(y_{max}) = 100\%$ and $\sum Q(y) = 100\%$

It is convenient to use the complementary CDF, or CCDF, i.e., $1 - CDF$ (sometimes called the "upper tail area") in the analysis of the envelopes of digital modulation schemes. CCDF expressed as a percentage is:

$$\text{CCDF} = 1 - Q(y) = 100 \times P[Y > y] \tag{11.13}$$

where y ranges over all values in Y. The CCDF has the following properties:

$$0 \leq 1 - Q(y) \leq 100\%;\ 1 - Q(y_{\max}) = 0\% \tag{11.14}$$

In a non-statistical peak power measurement the PAPR is the parameter which describes the headroom required in linear amplifiers to prevent clipping or compressing the modulated carrier. The meaning of this ratio is easy to visualize in the case of simple modulation in which there is close correspondence between the modulating waveform and the carrier envelope. When this correspondence is not present, the PAPR alone does not provide adequate information. It is necessary to know what fraction of time the power is above (or below) particular levels. For example, some digital modulation schemes produce narrow and relatively infrequent power peaks which can be compressed with minimal effect. The peak-to-average ratio alone would not reveal anything about the fractional time occurrence of the peaks, but the CDF or CCDF clearly show this information. The CCDF can be used to determine optimum transmitter power output and is also used to evaluate the various modulation schemes considered, to determine the demands that will be made on linear amplifiers and transmitters and the sensitivity to non-linear behaviour.

11.4 CCDF RESULTS FOR DIFFERENT WCDMA MODULATION CONFIGURATIONS

The PAPR CCDF of three WCDMA modulation techniques are presented in this section, namely the CCDF of conventional QPSK-modulated CDMA, as well as two versions of a patented WCDMA modulation technique employing constant-envelope root-of-unity filtered complex spreading sequences (CE-RU-CSS), denoted by 1/2C and 1C, respectively. The 1/2C WCDMA scheme, which features a perfectly constant signal envelope after modulation, produces a data throughput rate equal to that of conventional QPSK-modulated WCDMA. 1C denotes a more spectrally efficient four-dimensional extension of 1/2C, employing only one CSS for every four dimensions.

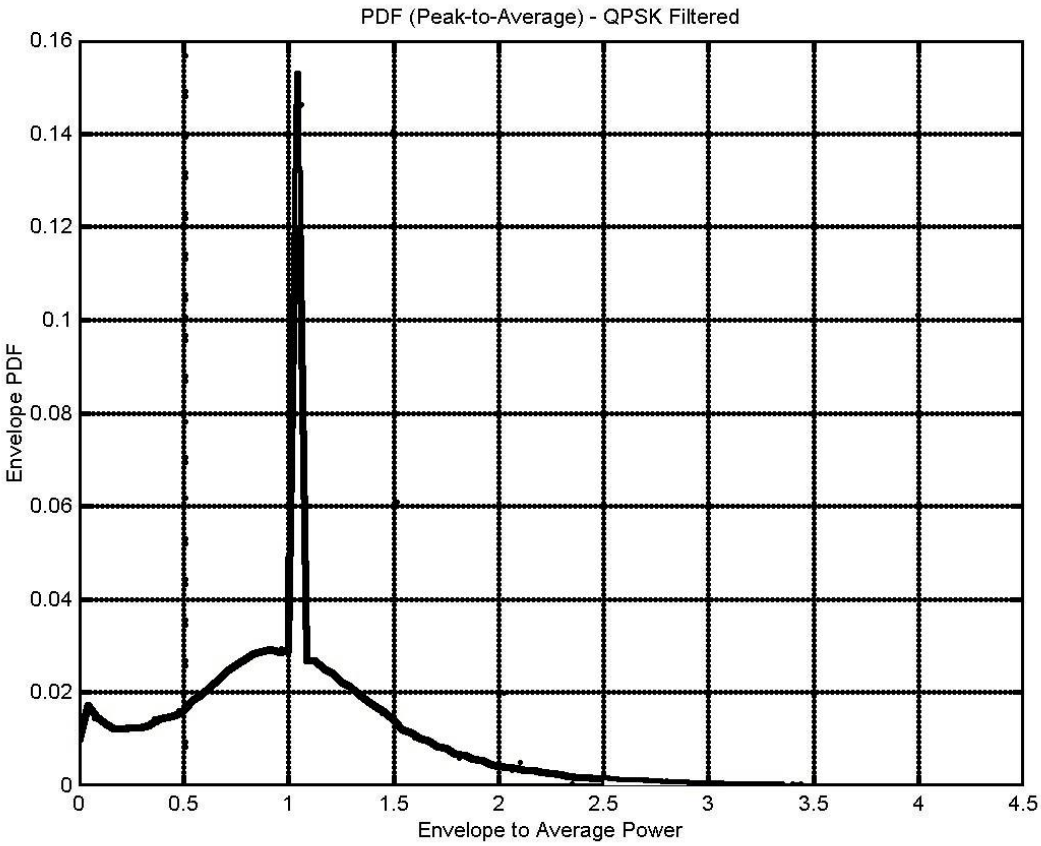

FIGURE 11.7: PDF of peak to average power ratio (PAPR) for QPSK

11.4.1 PAPR-CCDF of Conventional Nyquist-filtered Non Constant Envelope QPSK

The PAPR PDF of conventional Nyquist-filtered QPSK is shown in Figure 11.7, and the corresponding CCDF in Figure 11.8.

On the abscissa of Figure 11.7, 1 dB represents the average of the peak-to-average power. This reference value is normalized to 0 dB in Figure 11.8. The PAPR is plotted in terms of decibels and only for values equal to or exceeding 0dB, since this is the range of power ratios that directly determines the required transmitter power amplifier power back-off. According to the graph peak-to-average power values of greater or equal to 4.1 dB occur less than 1% of the time.

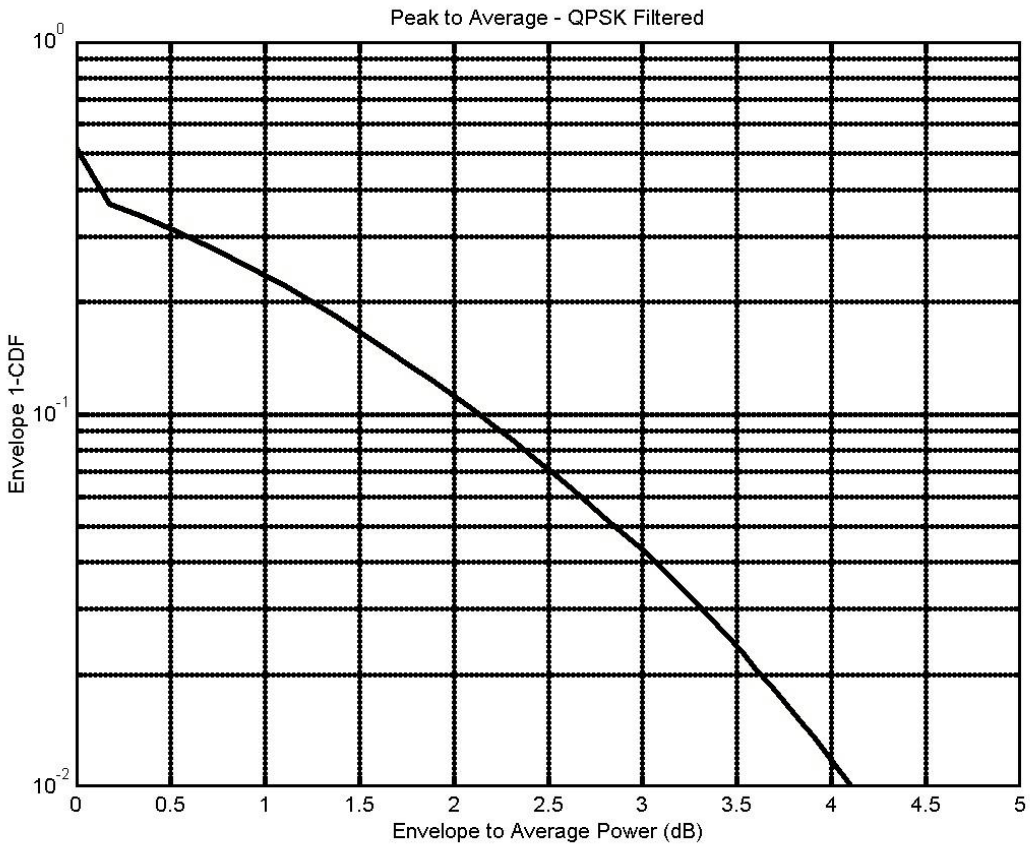

FIGURE 11.8: CCDF of peak to average power ratio (PAPR) for QPSK

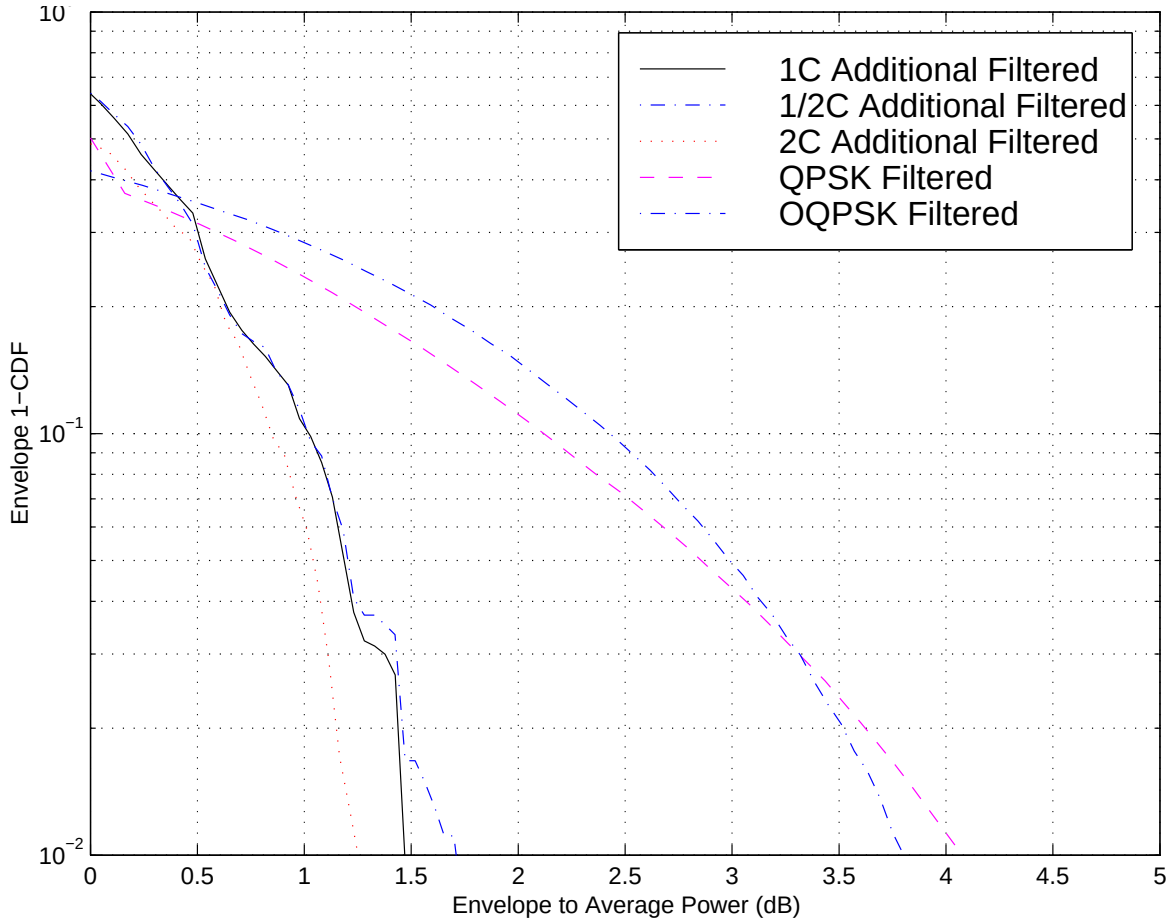

FIGURE 11.9: Peak-to-Average Power Ratio Complementary Cumulative Probability Distribution Function (PAPR-CCDF) measurements for CE-RU-filtered 1/2C and 1C modulated WCDMA, compared to conventional Nyquist-filtered QPSK-modulated WCDMA

11.4.2 PAPR-CCDF of Constant-Envelope 1/2C and 1C WCDMA modulation schemes

Figure 11.9 compares the PAPR-CCDF measurements of CE-RU-filtered 1/2C and 1C WCDMA modulation configurations, with a Nyquist filtered QPSK reference system.

In the case of the 1/2C modulation scheme it is clear that most of the power is contained in the peak-to-average power range of 1 to 1.2 dB. Before any additional filtering is applied, the instantaneous power envelope is totally constant and the PDF is only a single value at a peak-to-average power of 1 dB. Additional filtering is necessary to band limit the output signal to fit a specified RF spectral mask. It is the additional filtering that causes the peak-to average power variation seen in Figure 11.9. PAPR values of greater or equal to 1.7 dB nevertheless occur less than 1% of the time. It is also observed from the figure that the 1C

WCDMA modulation scheme exhibits PAPR values of greater or equal to 1.47 dB less than 1% of the time, which is only slightly worse than for 1/2C, but at twice the data throughput rate of conventional QPSK and 1/2C.

A direct comparison between the PAPR-CCDF measurements of the said modulation schemes reveals a 90-percentile peak-to-average power ratio advantage of approximately 2.15 and 2.2 dB for 1/2C and 1C, respectively, relative to QPSK under identical operating (filtering) conditions. Note the small but remarkable statistical PAPR power advantages gained by the 1C multi-dimensional CE-RU-filtered WCDMA modulation scheme relative to the perfectly constant envelope 1/2C configuration (approximately 0.25 dB), as well as the large improvement (approximately 2.5 dB) on the Nyquist filtered QPSK reference system.

11.5 POWER SATURATION PERFORMANCE OF MODULATION STANDARDS: EXPERIMENTAL TEST SETUP

Figure 11.10 gave a schematic representation of the 1 dB compression point of a power amplifier. The 1 dB Power Amplifier (PA) saturation point is defined as the point **A** where the low noise amplifier characteristic (solid graph) deviates 1 dB from the ideal linear amplifier power saturation curve (dashed graph). It serves as a reference point for both the PAPR-CCDF tests performed on the output signal of GSM and WCDMA modulation systems, as well as to different modulation schemes when subjected to non-linear power amplification and saturation.

The experimental test setup for non-linear power amplification (hard limiting) and power amplifier saturation measurements is shown in Figure 11.10. A Mini-Circuits ZFL-1000LN low noise amplifier (LNA) was used to perform the amplifier saturation tests presented.

The cdma2000 modulation schemes investigated in this report were all implemented on a generic FPGA development platform containing four Altera 600k FPGA devices. These configurations comprise a conventional Nyquist filtered QPSK CDMA reference transmitter, as well as three multi-dimensional WCDMA modem transmitter configurations (referred to as 1/2C and 1C) employing constant envelope root-of-unity filtered complex spreading sequences (CE-RU-CSS). A variable rate pseudo-noise (PN) generator, with length $N = 2^{48} - 1$, provides a serial random data input stream to each modem. The FPGA development platform produces the in-phase (I) and quadrature (Q) baseband signals of individual transmitter configurations. These digital I and Q channel outputs are then digital-to-analog converted, low-pass filtered and amplified, prior to modulation onto 250

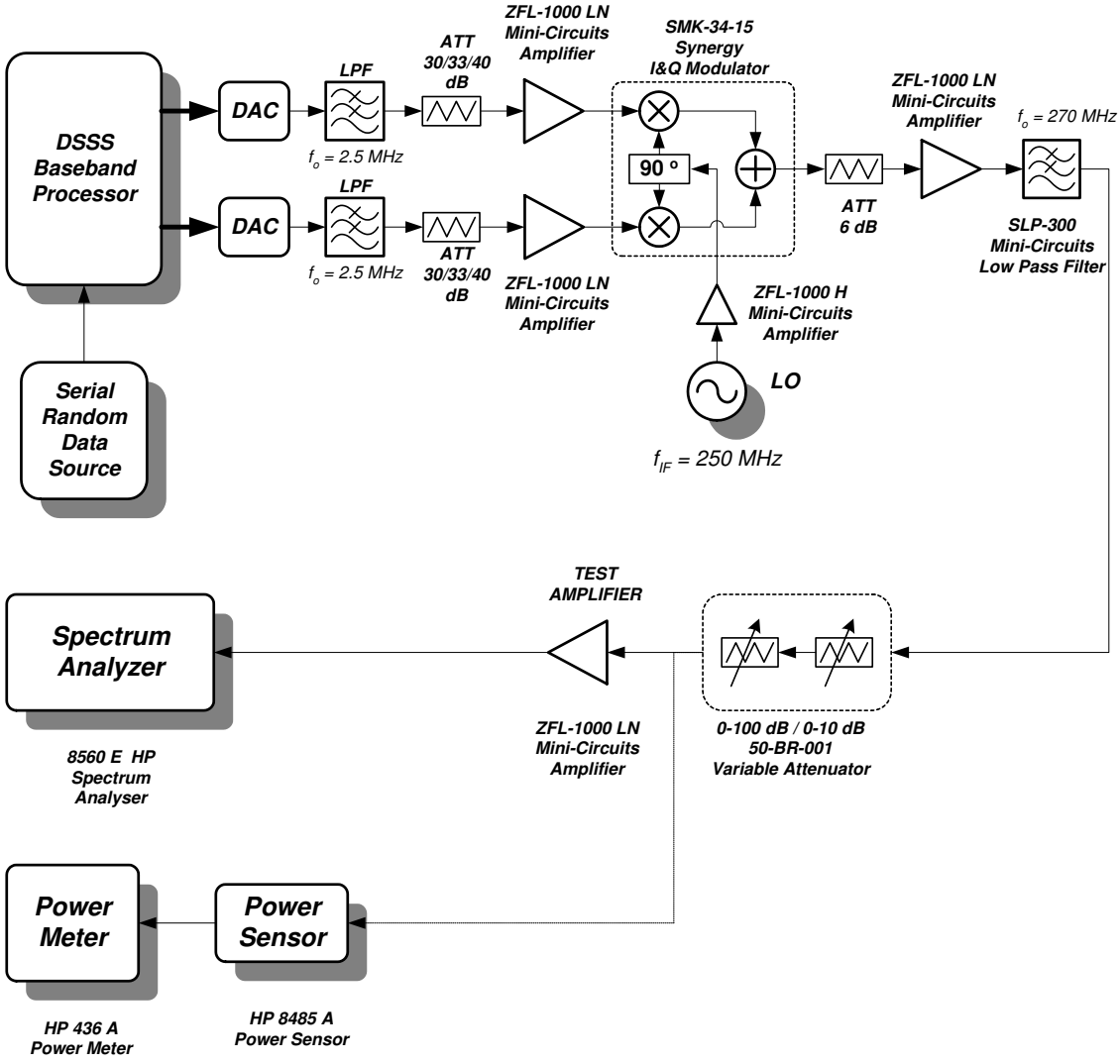

FIGURE 11.10: Block diagram of the power amplifier saturation test setup

MHz intermediate quadrature carrier frequencies.

The resultant modulated signal is then amplified and low-pass filtered to eliminate any unwanted, out-of-band harmonic components that may have been produced by the I&Q modulator. A variable attenuator is used to adjust the power level to the input of the *TEST AMPLIFIER* in 1 dB increments. Quadrature modulation and summation is done by means of an I&Q modulator and summer (Synergy, SMK-34-15). A properly calibrated HP 8485A power sensor and HP 436A power meter combination were used to perform all power measurements. Spectral measurements were done with a HP 8560E spectrum analyzer.

11.6 POWER SATURATION TEST RESULTS

The results presented below present spectral measurements under varying power saturation conditions performed on the proprietary 1/2C and 1C WCDMA modulation schemes and a standard QPSK-modulated WCDMA modulation scheme resembling the 3GPP WCDMA standard pilot channel. Both modulators comprise identical spreading (chip) rates and Nyquist baseband filtering to achieve the desired 3GPP 5 MHz RF spectral mask.

11.6.1 PSD Benchmarks

Figure 11.11 depicts the Power Spectral Density (PSD) of the Nyquist filtered QPSK modulated WCDMA reference system at a power amplifier input level of 20 dB below the 1 dB saturation point.

In contrast, Figure 11.12 depicts the PSD of the unsaturated CE-RU-filtered 1/2C WCDMA system at identical data and spreading rates, with additional filtering added to meet the specified RF spectral mask. Note that the attenuation at the ± 3 MHz (relative to the carrier) passband edges is 40.99 dB down relative to the signal level at the passband center, which is more than 10 dB better than the QPSK reference system in Figure 11.11.

Figure 11.13 shows the PSD of the Nyquist filtered QPSK modulated WCDMA reference system with the power amplifier input level at 2 dB below the 1 dB PA compression point. This result can be compared to the PSD of CE-RU-filtered 1/2C-modulated WCDMA with the power amplifier input level also set at 2 dB below the 1 dB compression point as illustrated in Figure 11.14.

The PSD of the Nyquist filtered QPSK modulated WCDMA reference system with the power amplifier input level at the 1 dB compression point and the PSD of CE-RU-filtered

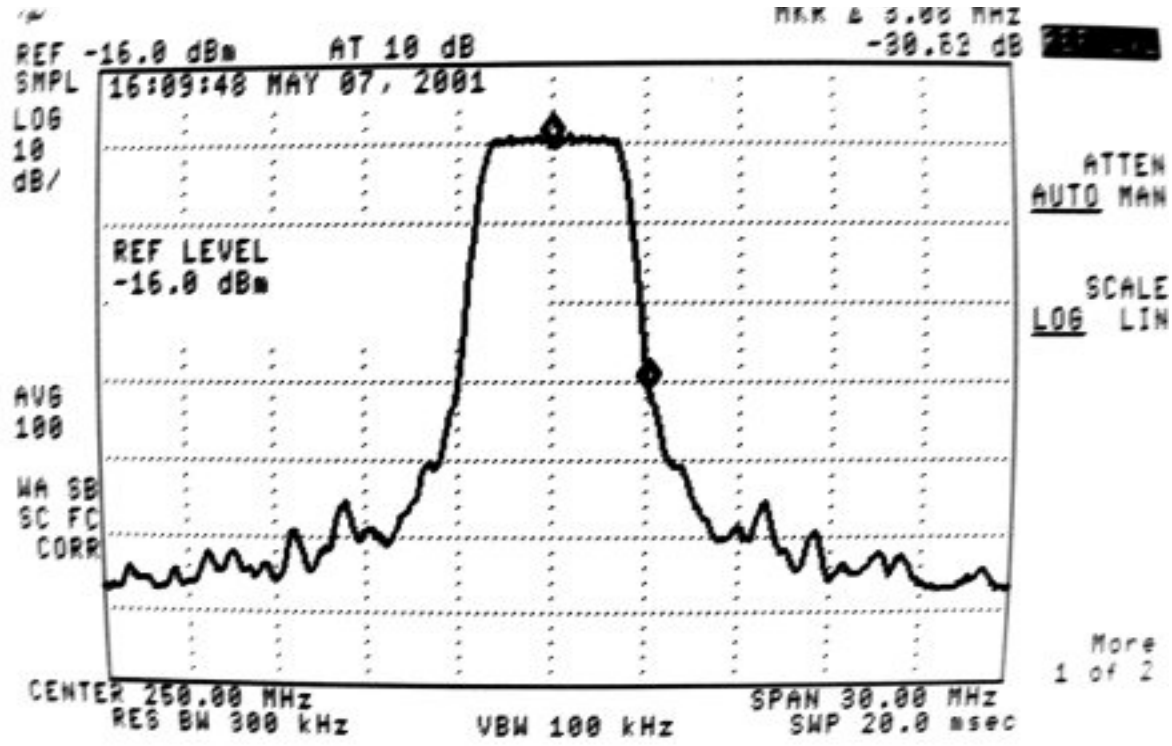

FIGURE 11.11: PSD of unsaturated Nyquist filtered QPSK modulated WCDMA reference system (power amplifier input level at 20 dB below the 1 dB PA compression point)

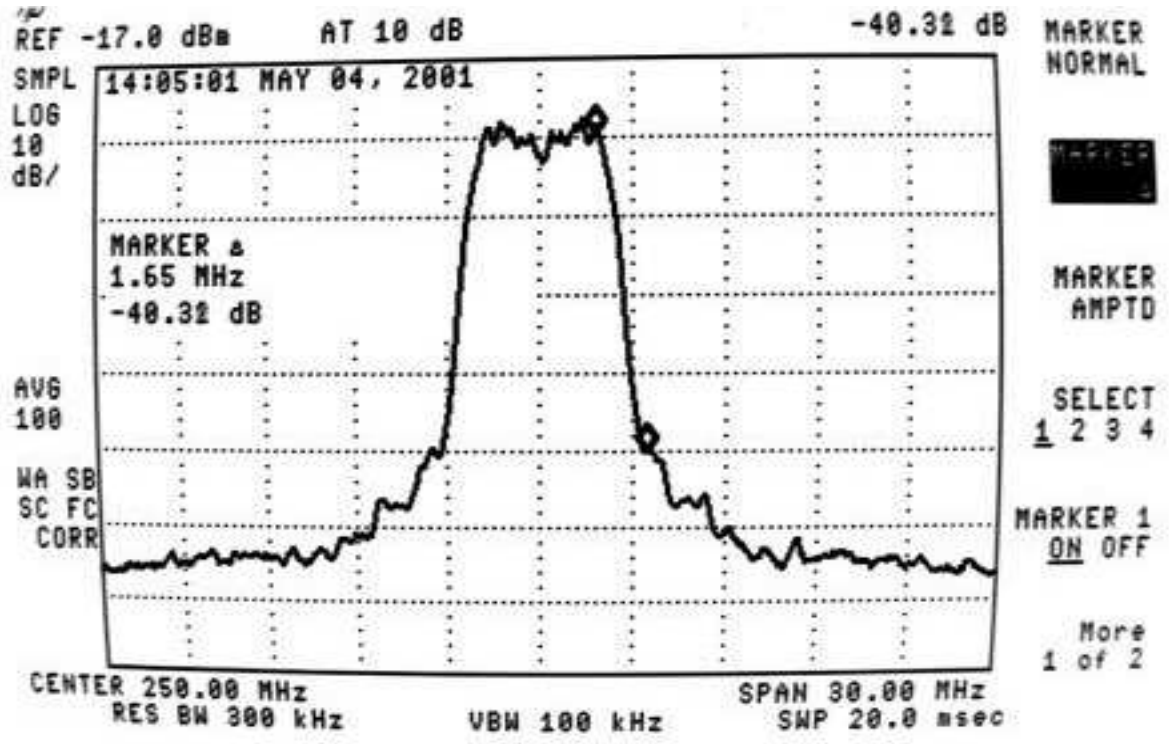

FIGURE 11.12: PSD of unsaturated CE-RU-filtered 1/2C-modulated WCDMA (power amplifier input level set at 20 dB below the 1 dB compression point).

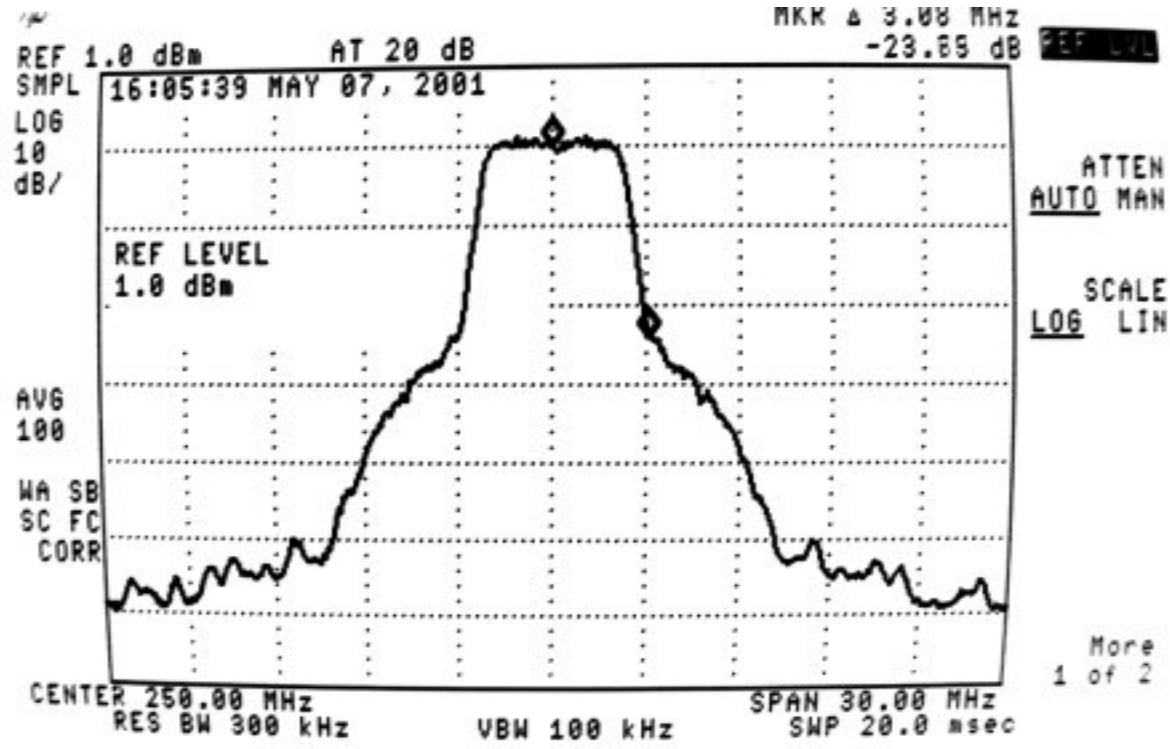

FIGURE 11.13: PSD of the Nyquist filtered QPSK modulated WCDMA reference system with the power amplifier input level at 2 dB below the 1 dB PA compression point

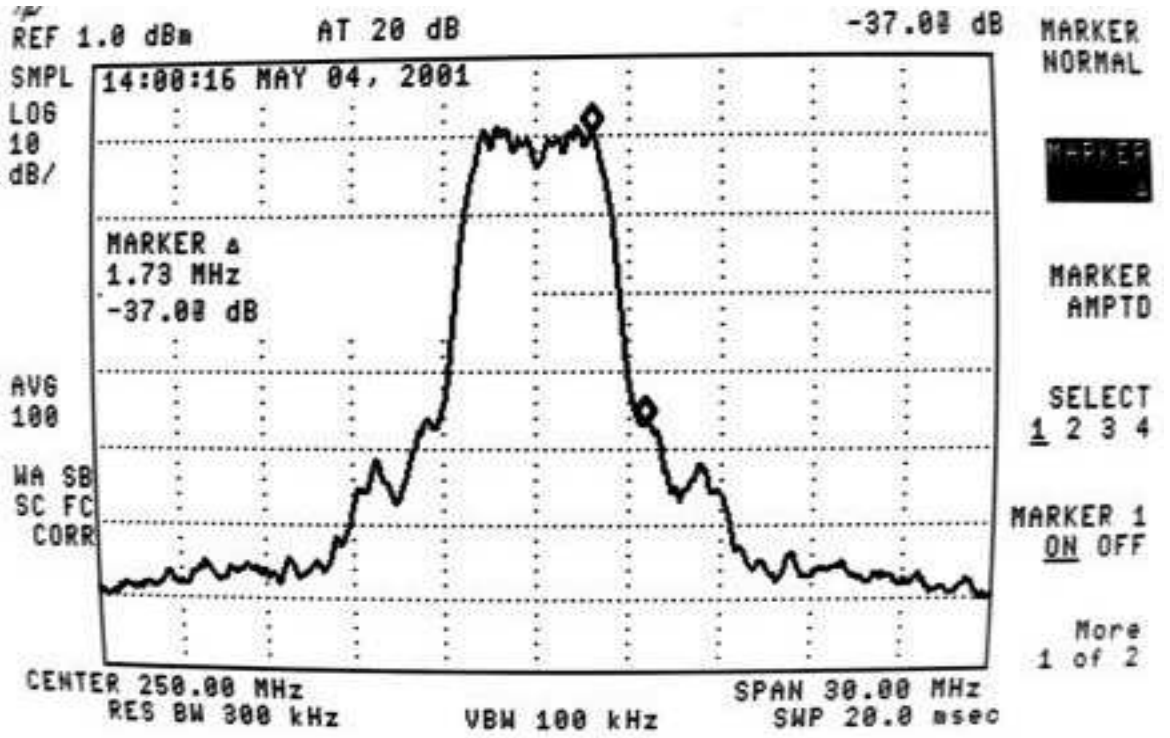

FIGURE 11.14: PSD of CE-RU-filtered 1/2C-modulated WCDMA with the power amplifier input level set at 2 dB below the 1 dB compression point

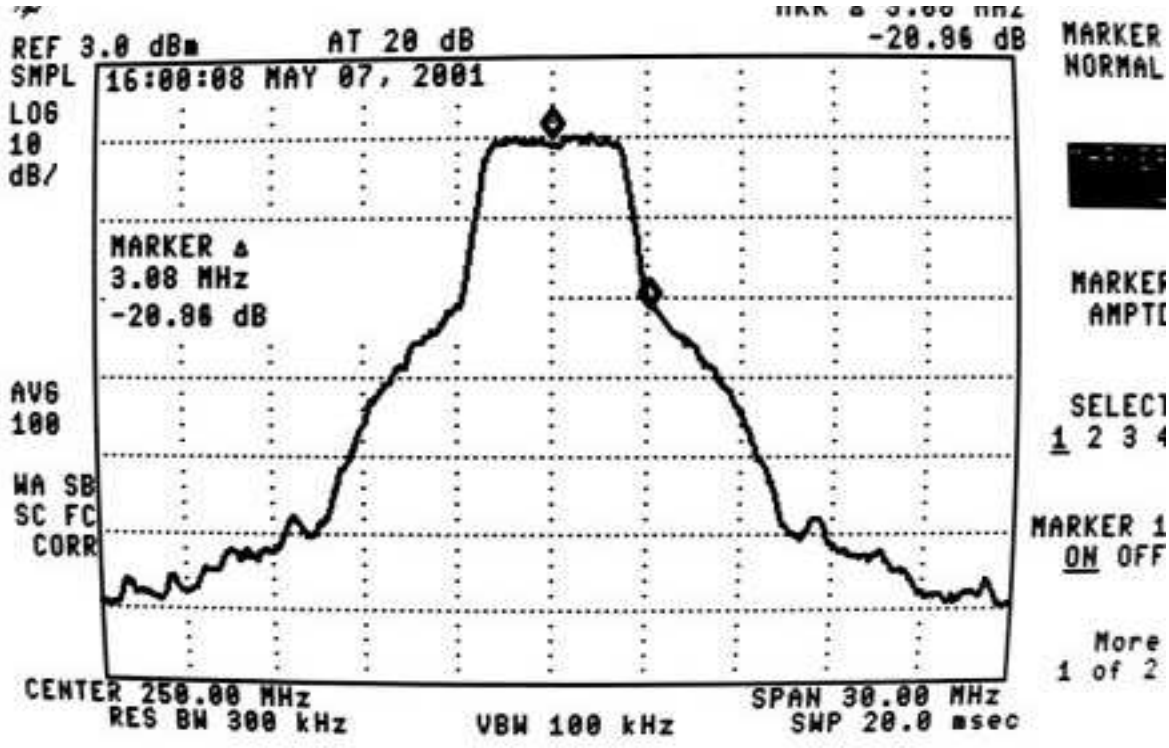

FIGURE 11.15: PSD of the Nyquist filtered QPSK modulated WCDMA reference system with the power amplifier input level at the 1 dB PA compression point

1/2C-modulated WCDMA with the power amplifier input level set at the 1 dB compression point are depicted in Figure 11.15 and Figure 11.16, respectively.

11.6.2 PSD of Modulation Schemes under Power Saturation Conditions

Spectral regrowth was investigated by comparing the power spectral densities of the various modulation schemes with a typical cdma2000 RF mask, as a function of the degree of amplifier saturation. The RF mask served as a benchmark to establish whether the spectral regrowth was within the excepted limits set by the mask. An attenuation of 30 dB relative to the nominal passband power level had to be achieved within a frequency span of 1.2 times the one-sided -3 dB transmission bandwidth $B/2$ centered on the IF carrier, where the cdma2000 bandwidth B is specified as 5 MHz for this application.

The spectral characteristics of each modulation scheme were monitored when the power amplifier was successively driven with input power levels of $-20, -10, -5, -3, -2, -1, 0, +1$ and $+5$ dB relative to the amplifier 1 dB compression point of -17 dBm. Only the -20 and -2 dB measurements are presented here.

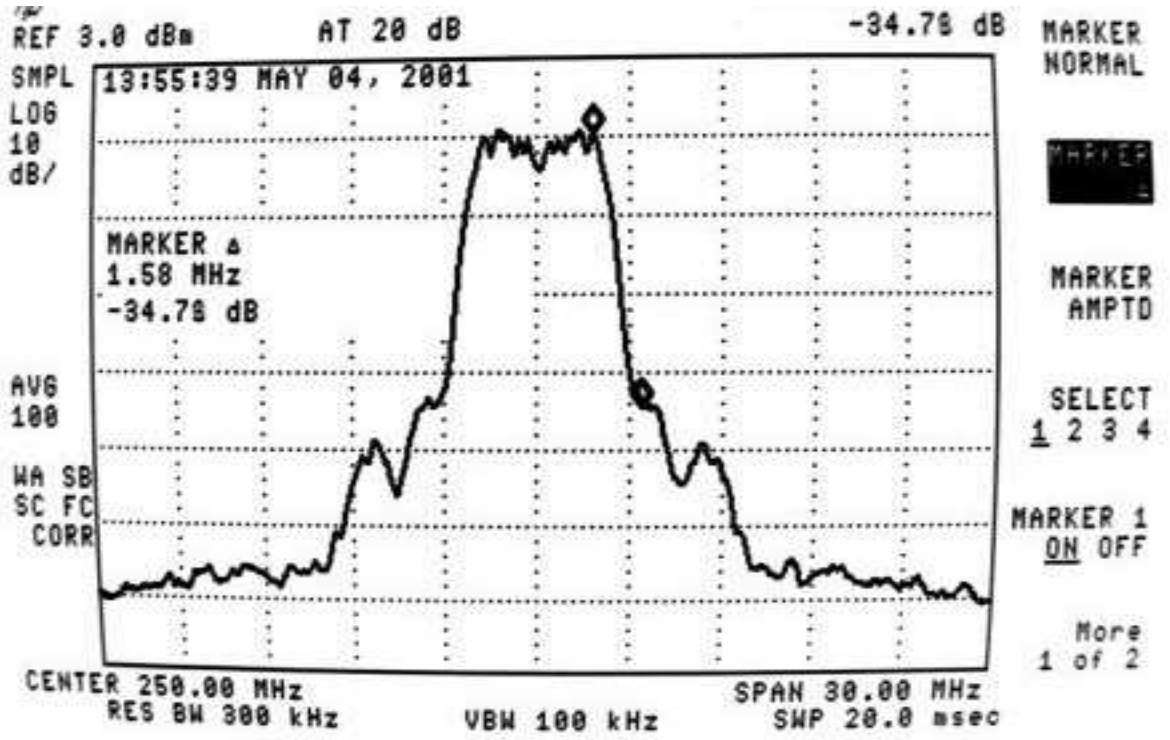

FIGURE 11.16: PSD of CE-RU-filtered 1/2C-modulated WCDMA with the power amplifier input level set at the 1 dB compression point

When the power amplifier is driven at a level of 2 dB below the 1 dB PA saturation point, the PSD of the Nyquist filtered QPSK reference system is attenuated by 23.85 dB at the ± 3 MHz passband reference frequencies, falling short of the specified required band edge attenuation of 30 dB by nearly 6 dBs. Significant spectral regrowth is thus evident in this particular case.

In the case of the constant-envelope root-of-unity (CE-RU) filtered 1/2C WCDMA modulation configuration the PSD attenuation at the 3 MHz band edges is only 38 dB when the power amplifier is driven at a level of 2 dB below the 1 dB PA saturation point. This represents an approximate 3 dB deterioration compared to the previous benchmark measurement depicted in Figure 11.12, but is more than 14 dB better than the QPSK reference system for the same PA input level. The corresponding attenuation for the 1C configuration is 32.09 dB relative to the nominal pass band power level, which easily meets the RF spectral mask requirement of 30 dB. Although this is nearly 6 dBs worse than 1/2C, it is still more than 8 dBs better than WCDMA spreaded Nyquist filtered QPSK. Note that this spectral confinement is achieved at *twice* the data throughput rate offered by both QPSK and the 1/2C WCDMA CE-RU filtered complex spreaded modulation schemes in a given spreading bandwidth.

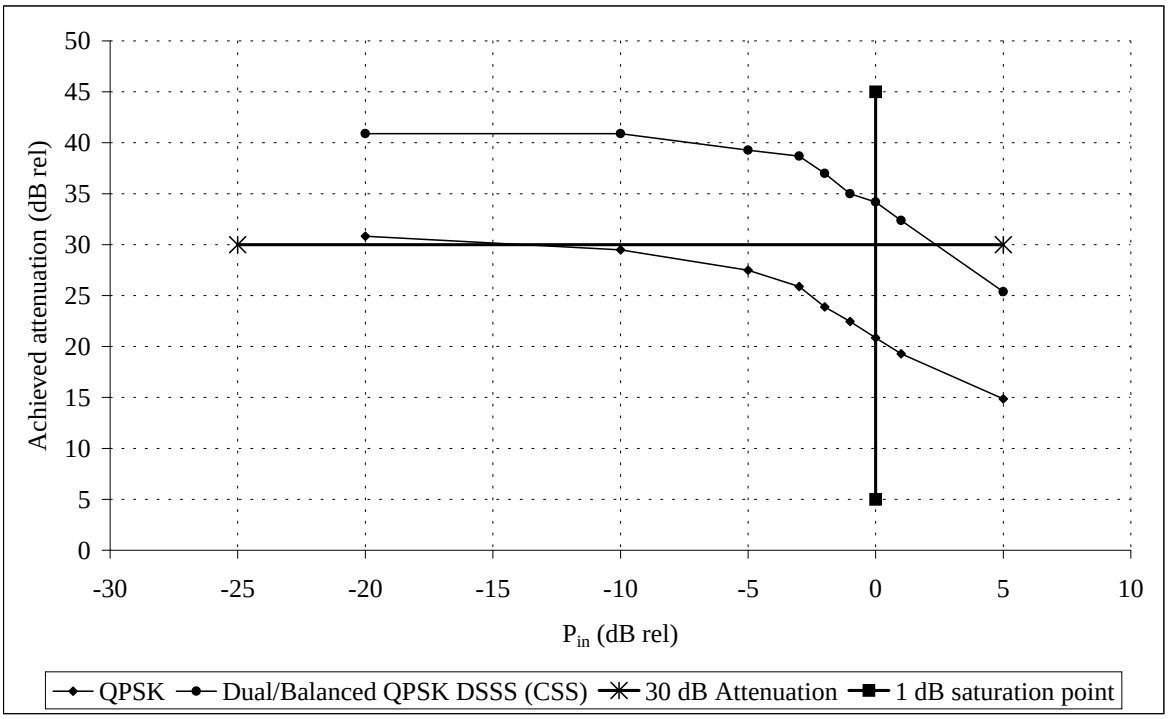

FIGURE 11.17: Graphical display of the spectral regrowth of the $\frac{1}{2}$C configuration CDMA system employing complex spreading sequences relative to a standard QPSK reference system as a function of power amplifier (PA) input level relative to the 1dB PA compression point.

The power saturation measurement results are summarized in Figure 11.17.

Table 11.1 compares the spectral regrowth results of the modulation schemes considered. The results indicate a relative advantage of several dBs for the 1/2C and 1C modulation schemes relative to QPSK in terms of the amount of power back-off required to operate within a specified RF mask and corresponding spectral regrowth limits.

Table 11.1: Summary of spectral regrowth of three modulation schemes based on P_{in} (dB) (Power amplifier input power level relative to the 1 dB PA compression point)

P_{in} (dB rel) Mod. Scheme	-20	-10	-5	-3	-2	-1	0	1	5
QPSK	30.82	29.49	27.48	25.89	23.88	22.46	20.86	19.28	14.86
Dual/Balanced DSSS QPSK (CSS)	40.89	40.98	39.28	38.68	37.00	35.00	34.18	32.38	25.38

11.7 CONCLUSIONS

With reference to Figure 11.9, a direct comparison between the PAPR-CCDF measurements of the said modulation schemes reveals 90-percentile peak-to-average power ratio advantages of approximately 2.15 and 2.2 dB for 1/2C and 1C, respectively, relative to QPSK under identical operating (filtering) conditions, but with data throughput rates in the ratio 1:2 compared to the QPSK reference system. A small but remarkable statistical PAPR advantage is noted for the multi-dimensional 1C WCDMA modulation scheme relative to the perfectly constant envelope 1/2C configuration (approximately 0.25 dB), as well as a large improvement (approximately 2.5 dB) on the Nyquist filtered QPSK reference system.

The relative PAPR CCDF measurement differences amongst the patented 1/2C and 1C WCDMA modulation schemes and the reference QPSK system depicted in Figure 11.9 exhibit remarkable correspondence with the relative power saturation and back-off hardware measurements which have been presented in Section 11.6. The results indicate that the QPSK modulation format must operate at a back-off of more than 10 dB (typically 14 dB) relative to the 1 dB saturation point in order to conform to the cdma2000 spectral mask at the 3 MHz, -30 dB attenuation reference points. The corresponding required back-offs for the proprietary 1/2C and 1C modulation schemes are 0 dB and -2 dB relative to 1 dB saturation point, respectively. In fact, no backup is required for the 1/2C modulator, which can operate well within the limits defined by the RF spectral mask at input levels up to 2 dB above the power amplifier 1 dB saturation point.

From the results presented it may be concluded that both CE-RU-filtered modulation schemes considered in this chapter have PAPR-CCDF and spectral regrowth advantages (measured in terms of how successful the RF spectral mask is met at the 3 MHz, -30 dB attenuation reference points) in the order of 12 to 16 dB over the standard QPSK reference system for power amplifier input levels in the range of -15 to +3 dB relative to the amplifier 1 dB saturation point. It should be emphasised that all the benefits in terms of spectral and power efficiency offered by all three CE-RU WCDMA modulation schemes are obtained while achieving uncoded bit error rate (BER) performances approximately equal (to within 0.5 to 2 dB) of the theoretical QPSK BER performance AWGN, as well as in Rayleigh fading, with data throughput advantages 1 and 2 for 1/2C and 1C, respectively, compared to the conventionally filtered WCDMA QPSK-modulated reference system.

CHAPTER TWELVE

ASPECTS FOR FUTURE RESEARCH AND CONCLUSION

12.1 ASPECTS FOR FUTURE RESEARCH

A wireless DSSS communication link was developed during the research and development study, comprising the various subsystems and exploiting the advantages and applications outlined in this dissertation. A two-dimensional hardware prototype evolved, consisting of a DSSS transmitter and receiver, employing complex spreading sequences. Novel carrier synchronization techniques, using novel sum and difference sequence combinations, were designed and analysed in order to overcome the presence of unwanted interference terms, generated in the process of achieving carrier phase estimation in the presence of complex spreading. Dedicated code tracking loops have been proposed, designed and analyzed, capable of tracking the chip timing of the desired received DSSS signal's complex spreading code within fractions of one chip period. The proposed new generic DSSS system is furthermore sufficiently versatile to allow the use of either binary or complex spreading sequences. Families of Non-Linearly-Interpolated Root-of-Unity (NLI-RU) filtered complex spreading sequences have been utilised, capable of producing constant-envelope Double-Side-Band (DSB), as well as Single-Side-Band (SSB) DSSS outputs. The generic DSSS system is very flexible in terms of data rate, spreading sequence length and Processing Gain (PG). Not only can different multi-phase as well as multi-amplitude modulation techniques be very easily implemented, but the system may also be easily adapted to serve various applications.

By virtue of the numerous possibilities and applications outlined for the prototype DSSS technology developed, a multitude of possible future research opportunities can be identified.

Different modulation extensions can be evaluated on the same platform. The system can be further evaluated in terms of different channel effects, etc. Additional digital signal processing (DSP) building blocks may be added to improve system performance. Typical building blocks are multi-user interference cancellation (MUIC), RAKE combining, forward error correction (FEC) coding, power control and equalisation. Although this dissertation concentrated on the application of CSS in two-dimensional modulation structures, extension of the principles to more dimensions (¿2) leaves scope for significantly advanced systems with improved spectral efficiency. The upwards-extendibility of the complex modulation concepts developed in this dissertation is a topic for future research.

12.2 CONCLUSION

The ultimate goal of this research project was to design and develop a generic DSSS modem employing complex spreading sequences (CSS). This objective has been achieved with the establishment of a prototype WLL RF-link, providing the required vehicle and test bed to verify and illustrate all the principles and concepts formulated, e.g., the concept of linear root-of-unity filtering and its realisation in hardware. The list of objectives outlined in the introductory part of the dissertation will now be reviewed briefly to illustrate what has been achieved, and the verify if all goals have been met.

The first objective was the theoretical design and analysis of a DSSS communication system employing complex spreading sequences. The theoretical analysis and design are presented in PART II of the dissertation, consisting of Chapters $2, 3, 4, 5$ and 6.

The second objective comprised the simulation of a DSSS wireless communication link employing complex spreading sequences. A complete system simulation was performed and all the results are depicted and described in PART III, consisting of Chapter 7 and 8, for the DSSS transmitter and receiver, respectively.

The design of implementation structures for the transmitter and receiver of a DSSS communication system with complex spreading sequences, employing appropriate (FPGA) implementation technologies forms the third objective. Different implementation technologies have been investigated and used in the hardware implementation of the transmitter and receiver structures. The system evolved from fast discrete FCT logic to the final Altera FPGA-based development platform on which the complete prototype system was finalised. Details of the hardware design and development are presented in Chapter 9 and 10.

The fourth objective comprised the design and realisation of implementation technologies for the synchronization of timing (code, bit and frame synchronisation), carrier frequency and phase estimation of a DSSS communication system employing complex spreading sequences. All the synchronisation subsystems have been implemented in reprogrammable FPGA hardware, resulting in the generation of considerable intellectual property (IP) in the form of additional DSSS/CDMA VHDL functional core software. These subsystems were all integrated as part of the final wireless DSSS modem link on the FPGA-based development platform. Chapter 10 contains the description and results of the final hardware DSSS modem transmitter and receiver prototype, utilising complex spreading sequences.

The final objective comprised the simulation and prototype hardware performance evaluation of the DSSS system under typical AWGN and some fading mobile channel conditions, including power saturation effects. The verification and performance evaluation of the implemented DSSS communication RF-link are presented in Chapter 11. Firstly the bit error rate (BER) performance was investigated. The BER performance of the hardware implemented differential encoded coherent balanced/dual DSSS modem is presented in Figure 11.1, and compared with the theoretical BER of QPSK and differentially encoded coherent QPSK. The hardware implementation loss of the DSSS system has been found to be in the order of $1.5\ dB$. This hardware implementation loss includes the losses due to the surface acoustic wave (SAW) bandpass filters, the non-linear effects of mixers in the transmission path, the effect of drifting and phase noise in all the local oscillators (LOs), etc. Considering all the impairments that have been included, the observed hardware implementation loss is relatively small. The system was simulated to investigate the effect of different phase errors on the BER performance. This simulation results are depicted in Figure 11.4 and is compared to the theoretical BER results of a QPSK system with different phase errors between transmit and receive carriers, presented in Figure 11.3. The simulated BER results correspond with the theoretical BER results for specific phase errors. System simulations were performed in a Raleigh-faded and AWGN channel. The simulated BER results obtained have been compared with the corresponding BER result of a theoretical QPSK system in an AWGN and Raleigh-faded channel, as shown in Figure 11.5.

Two specifications have been identified to evaluate the power amplifier saturation performance of the DSSS system. The first specification verifies if the output spectrum meets a specific RF mask specified for the transmitter output power spectrum. The second

verification test establishes whether a certain required bit error rate performance is achieved under power saturation conditions. The power efficiency of modulation schemes are usually measured in terms of the peak-to-average power ratio (PAPR) characteristics exhibited by the modulator output signal. Constant envelope modulation schemes exhibit very little, if any, spectral regrowth under non-linear amplification (saturation). Thus, with a constant envelope modulation communication system, larger power efficiency may be achieved by allowing the power amplifier to operate closer to the amplifier 1dB saturation point, without causing excessive spectral regrowth. It was found that the proposed constant envelope (CE) DSSS communication system employing complex spreading sequences passed both power saturation tests and outperformed binary DSSS systems employing Nyquist filtering, yielding non-constant envelope outputs. The power saturation evaluation results are presented in Chapter 11, with associated summaries given in Table 11.1 and Figure 11.17, respectively.

As a final example, an appropriately adapted version of the wireless DSSS communication system proposed in this dissertation, employing complex spreading sequences, was in fact utilised for a specific commercial application. The particular application comprised a long distance ($>$ 200 km) ultra wide-band DSSS equivalent of the prototype DSSS system, capable of meeting all the stringent requirements specified for this project, including low probability of interception (LPI) operation and synchronisation in the presence of adverse (sub-zero dB SNR) conditions. This project provided the final verification of the integrity of the results presented in this dissertation, and also illustrated the versatility and applicability of the concepts proposed, developed and presented during this research programme.